2021 10th International IEEE/EMBS Conference on Neural Engineering (NER)
Virtual Conference, May 4-6, 2021

Application of Digital Image Analysis Methods for Quantifying Spatiotemporal Neural Dynamics from Planar Microelectrode Arrays

Afareen Jaleel, Pawel Kudela, and William S. Anderson

***Abstract*—Recent developments in the ability to measure neural activity including surface and penetrating microelectrode arrays have allowed for higher-resolution and higher-dimension measurements of neural activity. With the development of this technology also arises the need for analytical methods to enable interpretation of these measurements in the context of underlying neural dynamics and processes. In this paper, we examine the application of methods such as current source density (CSD), histogram correlation, and radial profile analysis for quantifying the spatiotemporal characteristics of neural dynamics in both simulated and recorded local field potential (LFP) data.**

Keywords—Image Analysis, Neuromodulation, Neuroinformatics, Neurostimulation, Neural Implants

I. Introduction

Neural activity can be highly nonlinear and nonstationary [1], particularly in response to electric stimulation. When analyzing nonstationary data recorded from cortical surface or planar depth electrode arrays, image-analysis methods may be helpful in quantifying, comparing and assessing various spatial and event-related changes in neural activity detected by these electrodes in the plane of a recording array. The application of image-analysis techniques to neural data analysis may include but are not limited to quantification and comparison between pre- and post-stimulation neural states, tuning parameters for brain stimulation, or calibration (error functions) of high-resolution computational models of cortical activity. Furthermore, since these methods do not require more than one time sample for their calculation, they may have potential application for low latency closed-loop control of neural activity.

II. Methods

A. Recorded intracranial electrocorticographic signals

Intracranial electrocorticographic (iECoG) signals were recorded from the inferior frontal gyrus of an adult epilepsy patient implanted with a subdural grid (8 x 8 elements, 2.3 mm diameter) embedded with a 4 x 4 microwire array (0.075 mm) (Fig. 1). The patient provided informed consent for these studies in compliance with Johns Hopkins Institutional Review Board requirements and the study was approved by the Johns Hopkins Institutional Review Board. Monopolar stimulation with biphasic pulses was delivered to a nearby grid macroelectrode (pulse width 0.3 ms, stimulating current 5 mA) at interstimulus intervals of 5 sec in two blocks of 50 trials. Microwire array elements recorded cortical responses pre and post single pulse electrical stimulation across cortical micro-domains located 4 to 8 mm away from the center of a stimulating macroelectrode. The signals from the microwires were collected at 30,000 samples/second (250 nV resolution) using the NeuroPort System (Blackrock Microsystems). Trials with artifacts (33) were excluded from analyses. Local field potentials (LFP) from the cortical surface recorded using planar surface microelectrode arrays (Fig. 1) represent aggregated activity of neurons in close proximity to the recording electrodes [2].

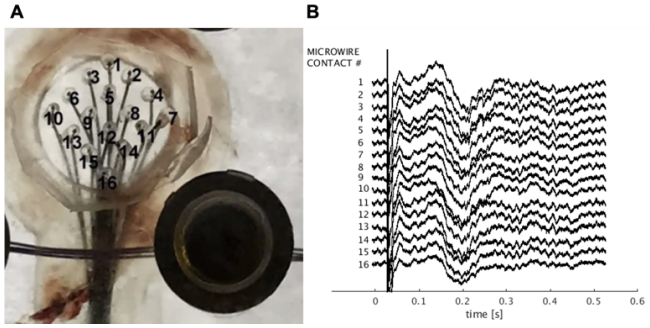

Fig. 1. A) Illustration of the 4 x 4 microelectrode array (0.075 mm diameter, 1 mm spacing) used to record local field potential data from the cortical surface along with the adjacent subdural grid contact (2.3 mm diameter) used for stimulations. B) Local field potentials recorded from the cortical surface.

B. Application of existing analytical methods: Kernel Current Source Density

Two-dimensional current source density (CSD) analysis of the LFP enables sensing of current flows in any direction within the plane of the microelectrode array. The 2D CSD is calculated using the formula $C = -\nabla(\sigma\nabla V)$ [3]. As shown in Fig. 2, 2D CSD profiles can be created from the LFP, and these profiles can be used to determine the location of current sources and sinks.

When comparing a cortical network operating in two states A and B, a simple distance metric derived from CSD values in A and B can be useful. The comparison between the two CSD profiles in *N* points at the plane of an electrode array, can be calculated according to the formula:

$$\sum \sqrt{(CSDA_{i,j} - CSDB_{i,j})^2} \ \ for\ i*j=N \qquad (1)$$

In the case of electrical cortical potentials recorded by a finite number of electrodes, calculation of (1) will require

This work was supported by U.S. Army Research Office grant #W911NF-20-1-0183.

Afareen Jaleel, Department of Biomedical Engineering, Johns Hopkins University, Baltimore, MD, U.S.A. (e-mail: ajaleel3@jhu.edu).

Pawel Kudela, MS, PhD, Department of Neurosurgery, Johns Hopkins School of Medicine, Baltimore, MD, U.S.A. (e-mail: pkudela@jhmi.edu)

William S. Anderson, MA, PhD, MD, Institute for Computational Medicine, Departments of Neurosurgery and Biomedical Engineering, Johns Hopkins School of Medicine, Baltimore, MD, U.S.A. (e-mail: wanders5@jhmi.edu)

2021 10th International IEEE/EMBS Conference on Neural Engineering (NER) | 978-1-7281-4337-8/21/$31.00 ©2021 IEEE | DOI: 10.1109/NER49283.2021.9441122

prior interpolation of values of electrical potential in points between the recording elements. To illustrate the sense of this metric, we used the Kernel Current Source Density package [4] to simulate three different datasets of local field potentials (LFPs) at the cortical surface resulting from three different current source density profiles (A, B, and C in Fig. 2). Using (1) to compare CSDs in A, B and C (N=10,000) the formula provides a value of 366 in the case of B and C, 633 in A and B, and 594 in A and C respectively. The lower the value of (1) the more similar the spatial distribution of LFPs and the corresponding CSD profile are. For instance, B and C have current sources and sinks on the upper and lower right respectively, whereas in A current sources and sinks are in the left upper and lower areas. Utilizing CSD instead of LFP values allows for localization of current sources and sinks and amplifies the similarities and differences of the profiles as indicated by the greater magnitude of values in the estimated CSD than LFP values in Fig. 2.

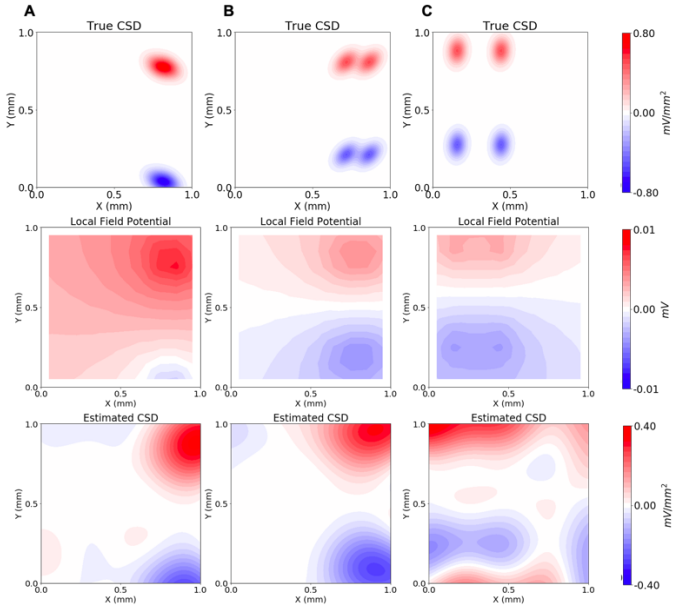

Fig. 2. A) Simulated LFP data for a surface microarray with one current source and one current sink with corresponding current source density profile below. B and C) Simulated LFP data with two current sources and two current sinks (note the different positions of current sources and sinks).

C. *Image analysis methods: Histogram Analysis and Correlation*

In digital image-analysis, image histograms allow classification and identification of image features, while the correlation of image histograms is used to quantify the similarity between images [5]. Histograms of local field potentials within the plane of the microelectrode array can be used to characterize the state of a cortical network. Electrical potentials are sampled by a finite number of electrodes at the cortical surface. To increase the LFP and histogram resolution, values of the potential at points between recording electrodes must be interpolated. Fig. 3 shows examples of contour plots of electrical potentials at the cortical surface sampled by a 4 x 4 microelectrode array after cubic spline interpolation. The histogram calculation and correlation functions are part of the OpenCV package [6], and the interpolation function is available in the SciPy package in Python [7]. As shown in Fig. 3, the image histogram profile can serve as a signature of LFP distribution, while the histogram correlation function in OpenCV can serve as a metric to quantify the similarity between two LFP distributions. For instance, the correlation between LFP histograms in Fig. 3(a) and 3(b) is 0.73, whereas the correlation between LFP histograms in Fig. 3(c) and 3(d) is 0.97.

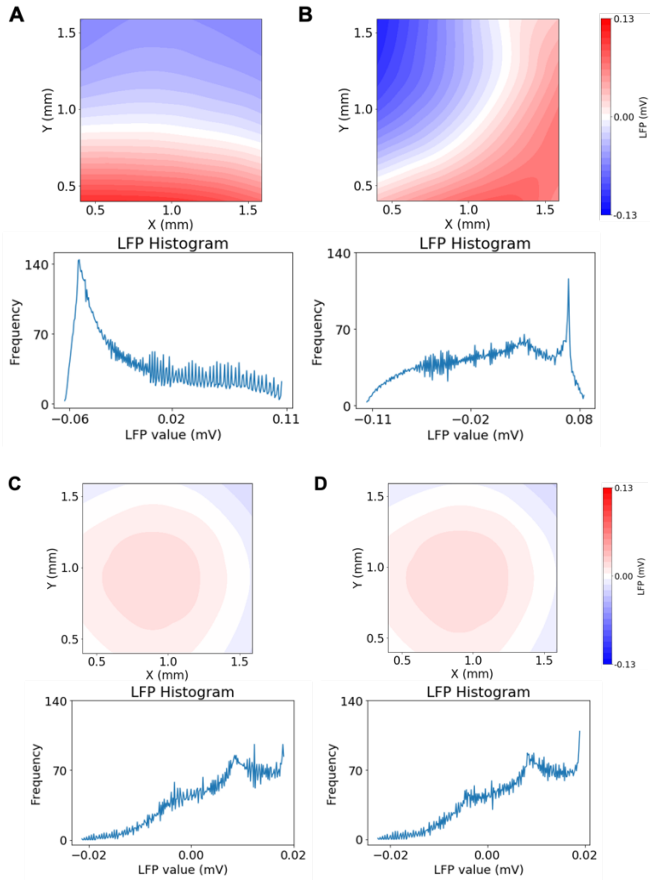

Fig. 3. Simulated LFP distributions and the corresponding LFP image histograms.

D. *The Radial Profile and Fourier Transform Analysis*

The Radial Profile (ImageJ [8] plugin) for analysis of microscopic images of biological specimens is used to assess the degree of cell/extracellular matrix co-alignment [9]. In its application to image analysis, the Radial Profile analyzes pixel values in a particular direction relative to a reference point in the center of an image. When applied to the 2D LFP distribution, this method can be used to sum electric potential values along the direction given by an angle θ ($0^\circ \leq \theta < 360^\circ$), relative to the point in the center of a planar array. The Radial Profile applied to the 2D Fourier Transform of an LFP distribution can sum the frequency of pixels of a particular magnitude relative to the center. This profile can be used for 2D "field mapping" of local field potentials in the plane of the microelectrode array. The azimuthally averaged electrical potentials plotted as a function of radius (0° - 360°) can provide useful information about arrangement and orientation of electric potential isolines within the plane of the microelectrode array and can be indicative of current

sources and sinks. The following analysis applications have been developed.

a) Radial Profile for Current Source Localization and Local Field Potential Comparison: The location of current sources and sinks in the plane of a microelectrode array can be estimated by finding the extreme values in the Radial Profile of the LFP distribution. For example, the positive peak in the LFP radial profile in Fig. 4(a) (bottom left graph) at the angle of 90° reveals the location of the current source, while the negative peak at the angle of 278° identifies the direction where the current sink exists. In another snapshot of the LFP recording shown in Fig. 4(b), the positive peak (current source) in the LFP Radial Profile is at an angle of 339°, whereas the minimum peak (current sink) at an angle of 172°. This shows that the Radial Profile applied to continuous LFP recordings can be useful for mapping of the current source-sink dynamics. As in the case of the CSD profile, the distance metric derived from the Radial Profile can be used to facilitate the comparison of two cortical network states as shown in Equation 2, or alternatively, the correlation coefficient between the two radial profiles can be calculated.

$$\sum_{\theta=0^{\circ}}^{360^{\circ}} \sqrt{(RPA_{\theta} - RPB_{\theta})^2} \qquad (2)$$

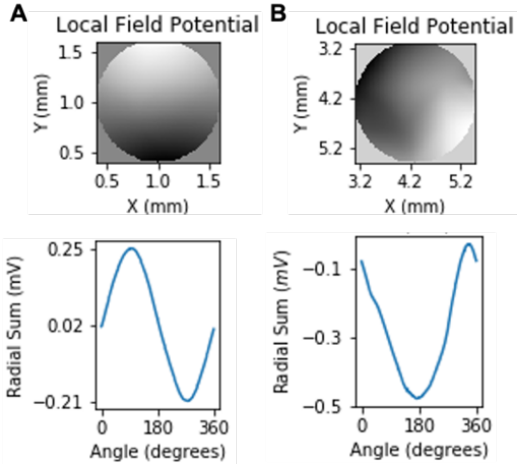

Fig. 4. A) Simulated LFP distribution with corresponding LFP Radial Profile. Lighter color indicates a more positive potential, whereas darker indicates a more negative potential. Areas outside the oval (circular) profile were excluded from analysis. B) Distribution of cortical LFP with the corresponding LFP Radial Profile.

b) Radial Profile for Current Source and Sink Counting: We used the Kernel Current Source Density package [4] to obtain three different datasets of LFP values at points in the simulated plane [3]. Each dataset was obtained from a different predefined number of spatially arranged current sources and sinks. The locations of current sources at the simulated plane and the matching LFP distributions are shown in Fig. 2. For each dataset, we obtained the Radial Profile of the LFP distribution (LFP radial profile). In addition, we applied a 2D Fourier Transform (FT) to each LFP distribution and computed the Radial Profiles of the matching 2D FT magnitude spectrum (FT radial profile). As shown in Fig. 5(a) and 5(b), the FT radial profile is more sensitive than the LFP radial profile in detecting multiple sources and sinks. However, as shown in Fig. 5(c), the FT profile is less precise in sensing the direction at which the current sources and sinks are located. Therefore, in the case of cortical surface or depth planar electrode recordings, the LFP radial profile may be used to determine locations of current sources and sinks at the plane of electrodes and the FT radial profile to determine the number of current sources and sink in regions of interest.

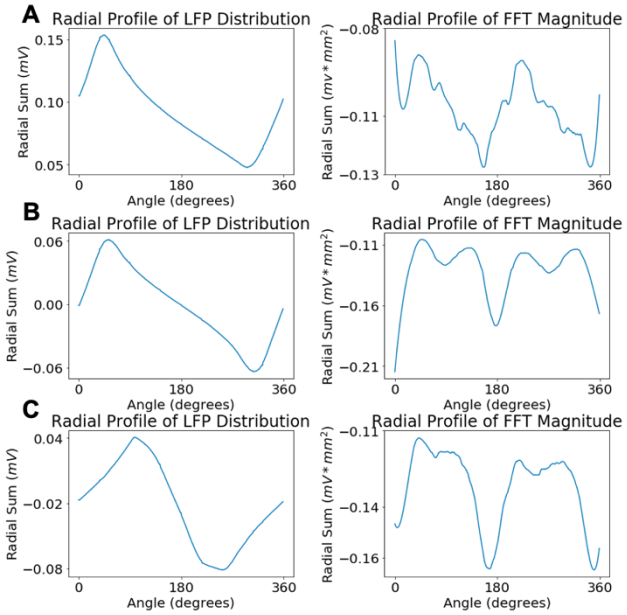

Fig. 5. Radial Profile of Local Field Potential, and Radial Profile of FT Magnitude Spectrum for the simulations from Fig. 2, i.e. (A) one current source and sink on right, (B) two current sources and sinks on right, and (C) two current sources and sinks on left

III. Results

To demonstrate the application of these image-analysis based methods in quantifying and comparing event-related changes in neural activity we used radial profiles to investigate the state-dependent response to cortical stimulation (or the context-dependent effects of stimulation). We used a data set of recorded iECoG signals sampled 100 ms prior, and after cortical stimulation from a patient with epilepsy. Heatmaps of radial profile correlations for the 67 paired pre- and post-stimulation cortical states based on LFP values are shown in Fig. 6. In the heatmaps (Fig. 6(a), 6(b)) similar radial profiles were indicated by darker squares whereas lighter squares were used to indicate dissimilar profiles. Given that the radial profiles were used to quantify cortical states these heatmaps demonstrated the existence of variability across cortical states before as well as after stimulation. In the heatmap in Fig. 6(b), variability among post-stimulation states suggests the possible state-dependent effect of stimulation while the high prevalence of correlated post-stimulation states, regardless of the number of correlated pre-stimulation states, would suggest a constant outcome for stimulation. Among the post-stimulation states in Fig. 6(b), 726 of 2211 (32%) pairs were correlated (> 0.5) whereas, in the case of the pre-stimulation states in Fig. 6(a), 603 of 2211 (27%) were correlated, respectively. The similar numbers of correlated states in both groups indicated the effect of electrical stimulation was state-dependent rather than constant.

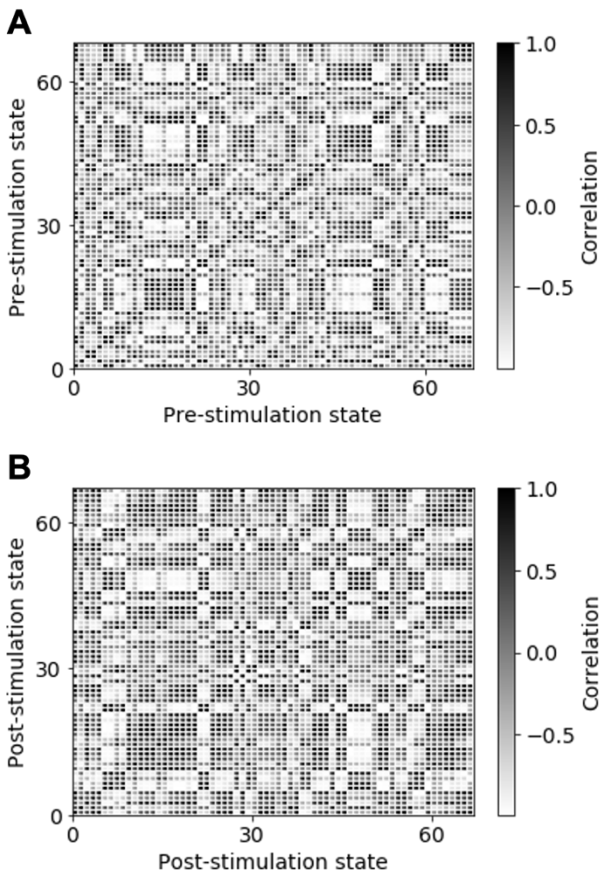

Fig. 7. Radial profile correlation heatmaps of (A) pre-stimulation and (B) post-stimulation states

To further prove this hypothesis, we defined criteria for evaluating the state-dependence of post-stimulation states (or cortical responses). State-dependence was defined as the conditional probability that pre-stimulation states were similar given the corresponding post-stimulation states were similar. We adopted a criterion that pre-stimulation states were defined as similar if the radial profile correlation was positive, and post-stimulation response radial profile correlation was greater than 0.9. A cortical response was classified as state-dependent if the conditional probability was greater than 0.7 from matching similar post-stimulation states with their corresponding pre-stimulation states. Based on this criterion, in the dataset, we found that 22 cortical responses were classified as state dependent. To assess the statistical significance of this result, we performed a permutation test by shuffling the order of pre-stimulation states. Thus, the null hypothesis of this test was that the pre-stimulation context does not affect cortical responses to stimulation, whereas the alternative hypothesis was that the pre-stimulation context affects the cortical response in this dataset. Under the null hypothesis (N=1000 permutations of pre-stimulation states) we found less state-dependent responses (with a mean of 13.9 and standard deviation of 3.4 across all permutations). The test yields a p-value of 0.01 and gave evidence in favor of the alternative hypothesis and against the null hypothesis since there was a higher number of 22 state-dependent states in the original dataset without permutation. The obtained result confirms that the pre-stimulation context contributes to the cortical response to stimulation. While this dataset has a small sample size, these results illustrate the potential of utilizing radial profiles and radial profile correlation in quantifying the effect of cortical stimulation. This methodology requires larger datasets to assess in detail the effect of stimulation on cortical activity.

IV. Conclusion

In this study, we proposed several methods for quantifying and comparing the spatiotemporal characteristics of neural activity measured with surface or penetrating planar microelectrode arrays. This included 2D current source density analysis and the image analysis methods, including histogram correlation and radial profiles. Application of a pointwise difference metric to compare current source density profiles allows for quantifying the similarity between neural states, particularly highlighting the differences in distribution of current sources and sinks. Likewise, histogram correlation can also be used to quantify similarities between neural states by comparing the spatial distribution of LFP values. Radial profile analysis can be used to parameterize the distribution of LFP values by an angle relative to the center of the microelectrode array. The radial profile can then be used in conjunction with signal analysis methods like the Fourier Transform to identify and count current sources and sinks, and thereby compare neural states. Lastly, based on the radial profile, we defined and applied comparison metrics to quantify the state-dependent effects of cortical stimulation.

References

[1] A. Ya. Kaplan, A. A. Fingelkurts, A. A. Fingelkurts, S. V. Borisov, and B. S. Darkhovsky, "Nonstationary nature of the brain activity as revealed by EEG/MEG: Methodological, practical and conceptual challenges," *Signal Processing*, vol. 85, no. 11, pp. 2190–2212, Nov. 2005, doi: 10.1016/j.sigpro.2005.07.010.

[2] S. Katzner, I. Nauhaus, A. Benucci, V. Bonin, D. L. Ringach, and M. Carandini, "Local origin of field potentials in visual cortex," *Neuron*, vol. 61, no. 1, pp. 35–41, Jan. 2009, doi: 10.1016/j.neuron.2008.11.016.

[3] J. Potworowski, W. Jakuczun, S. Łęski, and D. Wójcik, "Kernel Current Source Density Method," *Neural Computation*, vol. 24, no. 2, pp. 541–575, Nov. 2011, doi: 10.1162/NECO_a_00236.

[4] C. Chintaluri, M. Kowalska, W. Sredniawa, M. Czerwinski, J. M. Dzik, J. Jedrzejewska-Szmek, and D. K. Wójcik, "kCSD-python, a tool for reliable current source density estimation," *bioRxiv*, p. 708511, Jul. 2019, doi: 10.1101/708511.

[5] S. Narayanan and P. K. Thirivikraman, "Image similarity using Fourier Transform," *International Journal of Computer Engineering & Technology (IJCET)*, vol. 6, no. 2, pp. 29–37, Feb. 2015.

[6] *OpenCV*. Open Source Computer Vision Library, 2015.

[7] K. J. Millman and M. Aivazis, "Python for Scientists and Engineers," *Computing in Science Engineering*, vol. 13, no. 2, pp. 9–12, Mar. 2011, doi: 10.1109/MCSE.2011.36.

[8] W. S. Rasband, *ImageJ*. Bethesda, Maryland, U.S.A.: U.S. National Institutes of Health, 1997–2018.

[9] S. E. Taylor, T. Cao, P. M. Talauliker, and J. Lifshitz, "Objective morphological quantification of microscopic images using a Fast Fourier Transform (FFT) analysis," *Current Protocols Essential Laboratory Techniques*, vol. 7, no. 1, p. 9.5.1-9.5.12, 2013, doi: 10.1002/9780470089941.et0905s07.